

# Teaching Humans Subtle Differences with *DIFFusion*

Mia Chiquier\*  
Columbia University  
mia.chiquier@cs.columbia.edu

Orr Avrech\*  
Columbia University  
oa2429@columbia.edu

Yossi Gandelsman  
UC Berkeley  
yossi.gandelsman@berkeley.edu

Berthy Feng  
California Institute of Technology  
bfeng@caltech.edu

Katherine Bouman  
California Institute of Technology  
klbouman@caltech.edu

Carl Vondrick  
Columbia University  
vondrick@cs.columbia.edu

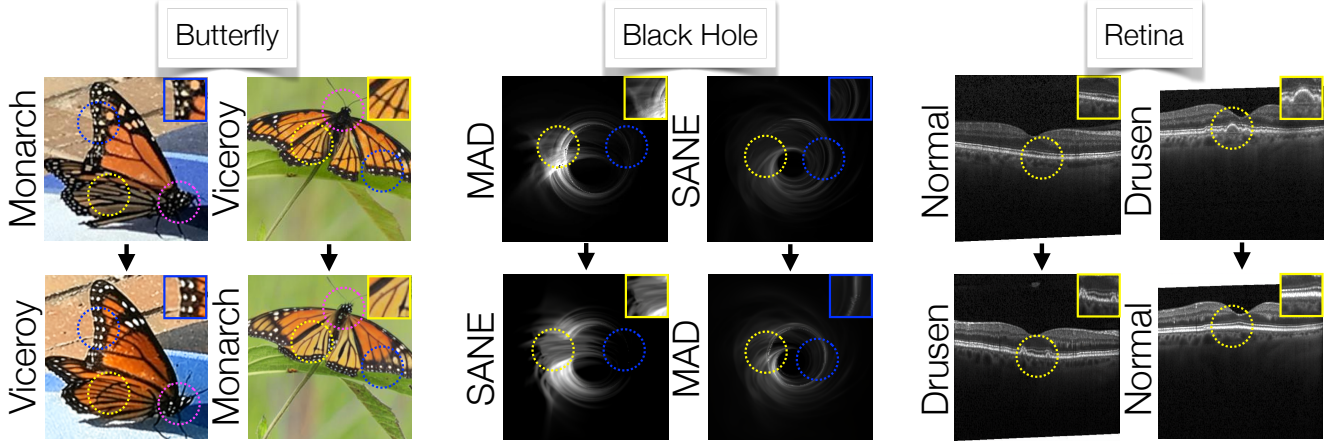


Figure 1. **DIFFusion Counterfactuals.** We illustrate the counterfactual results from our methods on the Butterfly dataset, the Black Hole dataset, and the Retina dataset. In the Butterfly dataset, the Viceroy has a cross-sectional line (yellow), a smaller head with less dots (magenta), and more “scaly” dots (blue), compared to the Monarch. In the Black Hole dataset, SANE has more uniform wisps (yellow) and less of a prominent photon ring (blue) as compared to MAD, with these distinguishing features discovered through our method rather than known a priori. In the Retina dataset, normal retinas lack the horizontal line bumps (yellow) present in retinas with drusen.

## Abstract

Human expertise depends on the ability to recognize subtle visual differences, such as distinguishing diseases, species, or celestial phenomena. We propose a new method to teach novices how to differentiate between nuanced categories in specialized domains. Our method uses generative models to visualize the minimal change in features to transition between classes, i.e., counterfactuals, and performs well even in domains where data is sparse, examples are unpaired, and category boundaries are not easily explained by text. By manipulating the conditioning space of diffusion models, our proposed method *DIFFusion* disentangles category structure from instance identity, enabling high-fidelity syn-

thesis even in challenging domains. Experiments across six domains show accurate transitions even with limited and unpaired examples across categories. User studies confirm that our generated counterfactuals outperform unpaired examples in teaching perceptual expertise, showing the potential of generative models for specialized visual learning.

## 1. Introduction

Generative models, especially large-scale image diffusion models, have transformed text-to-image creation, opening new ways to visualize concepts across various do-

\*Equal contribution.

mains. These models can produce counterfactual images—edits that shift an image from one category to another while preserving its identity—through text-guided editing or classifier-based techniques. To date, such efforts have centered on everyday domains with clear category distinctions, like cats versus dogs, rather than scientific fields such as medical imaging or astronomical classification. In these specialized areas, subtle visual differences are harder to detect, making counterfactuals particularly valuable for enhancing visual learning.

However, applying counterfactuals to specialized domains presents significant challenges. While effective in familiar contexts, counterfactuals struggle in scientific fields where training data is scarce and lacks paired examples showing corresponding features across categories. Text-based editing often fails to capture the precise visual nuances critical in these domains. These challenges are compounded by practical limitations—collecting comprehensive datasets requires specialized expertise and access to restricted equipment or subjects. This combination of limited data representation, unpaired examples, and complex domain-specific variations necessitates novel approaches for effectively leveraging generative models as teaching tools in specialized fields.

Current approaches highlight these limitations. Text-guided editing methods rely on linguistic descriptions, which can be too ambiguous to specify desired visual changes. Methods like Concept Sliders’ [15] effectiveness depend on paired examples in most cases—a constraint limiting their use in teaching scenarios. Visual counterfactual generation methods often require training a classifier, a limitation when data is scarce. Even classifier-free alternatives, like TIME [25], struggle with image quality and coherence for subtle differences.

We propose a framework that teaches visual concepts by generating natural transitions between categories, using class image distributions. Our approach leverages diffusion models’ priors to edit images, smoothly interpolating between categories while preserving instance-specific features without paired data or linguistic descriptions. We achieve this via targeted manipulations in the conditioning space, capturing nuanced transitions and image structure. This allows meaningful transformations from few examples per category, fitting specialized domains with limited data.

Through experiments across six domains, we demonstrate our approach’s effectiveness and utility. We highlight results on medical imaging (retinal diseases) [28], astronomical data (black holes), and natural domains (butterflies), each posing unique challenges in visual expertise training. Our method achieves better reconstruction quality and more coherent transformations compared to existing approaches, with high-quality results from limited data. User studies confirm that our transformations help people

distinguish categories more effectively. By generating nuanced counterfactuals in data-scarce specialized domains, our framework bridges the gap between generative modeling and visual expertise training, paving the way for broader applications in scientific education and discovery.

## 2. Related Work

**Visual Counterfactual Explanations.** A counterfactual image shows how an input would appear if altered to switch its class, enhancing interpretability. Counterfactual inference crafts images that not only differ in classification but also clarify the visual features defining each distribution. Approaches for visual counterfactual explanations (VCEs) make use of generative model edits, with VAEs [42], GANs [30], and more recently, diffusion-based methods [3, 13, 23–25, 48]. Most diffusion-based approaches adapt classifier guidance [11] to steer the generative process of counterfactuals, requiring access to the classifier and test-time optimization to produce counterfactual images. However, generating counterfactuals this way can be challenging, as the optimization problem closely resembles that of adversarial examples. TIME [25] proposes an alternative approach by using Textual Inversion [14] to encode class and dataset contexts into a set of text embeddings, providing a black-box framework for counterfactual explanations. While this removes the need for direct classifier access, Textual Inversion is primarily designed for personalization, focusing on regenerating concepts in novel scenes rather than preserving image structure—an essential aspect of counterfactual generation.

**Image Editing.** Recent advances in text-to-image diffusion models [29, 37, 40, 43, 45] have enabled test-time controls for image editing, ranging from semantic modifications to attention-based edits and latent space manipulation. Early approaches applied noise to an image and then denoised it using a new prompt [35], but this often resulted in significant structural changes. Later methods refined direct prompt modifications by incorporating cross-attention manipulations or masking to better preserve image structure [4, 9, 18, 39, 51]. Brooks *et al.* [5] use controlled edits from these methods to train a new diffusion model based on instruction-driven prompts. However, these approaches are limited to text-driven modifications, which restrict the flexibility of edits beyond what can be described with text. Unlike single-image editing methods, Concept Sliders [15] introduce a different approach by optimizing a global semantic direction across the diffusion model. While text pairs can guide their optimization, they also propose visual sliders based on image pairs. However, the visual slider approach struggles with unpaired data.



**Diffusion Models with Image Prompts.** Text-to-image diffusion models generate images from text prompts, but text often falls short in capturing nuanced concepts. Image prompts offer a richer alternative, conveying nuanced details more effectively, as "a picture is worth a thousand words." DALL-E 2 [40] pioneered this by conditioning a diffusion decoder on CLIP image embeddings, aided by a diffusion prior for text mapping. Later works offer different architectures [41] or adapt text-to-image models for image prompts [2, 16, 29, 57].

**Diffusion Inversion.** Editing a real image typically requires first obtaining a latent representation that can be fed into the model for reconstruction. This latent representation can then be modified, either directly or by altering the generative process, to produce the desired edit. Most diffusion-based inversion methods rely on the DDIM [49] sampling scheme, which provides a deterministic mapping from a single noise map to a generated image [36, 39, 53]. However, this approach introduces small errors at each diffusion step, which can accumulate into significant deviations, particularly when using classifier-free guidance [19]. Instead of predicting an initial noise map that reconstructs the image through deterministic sampling, an alternative approach considers DDPM [20] sampling and inverts the image into intermediate noise maps [55]. Building on this, Huberman-Spiegelglas *et al.* [22] proposed an inversion technique for the DDPM sampler, along with an edit-friendly noise space better suited for editing applications. In our work, we utilize this technique, while conditioning on image prompts.

**Machine Teaching.** Machine teaching optimizes human learning via computational models. Early work framed this as an optimization task, minimizing example sets for efficient teaching [59]. Generally, the field of machine learning for discovery has machine teaching as a goal [6, 27]. Recent advances leverage generative models and LLMs for cross-modal discovery, synthesizing representations for conceptual learning [7], decoding structures in mathematics, or programs for scientific discovery [34, 44]. Parallel efforts amplify subtle signals for perception: language models detect fine-grained textual differences [12], while video motion magnification enhances visual cues [32, 38, 56]. These methods, though effective for fine-grained discrimination, typically require aligned, abundant data and focus on single modalities. Our work extends these efforts, using diffusion models to generate visual counterfactuals for nuanced category learning.

### 3. Method

We begin by introducing *DIFFusion* for counterfactual image generation, as illustrated in Figure 2. In Section 3.1, we

provide the necessary background on diffusion models. In Section 3.2, we present our proposed method, outlining its design and implementation.

#### 3.1. Diffusion Preliminaries

Diffusion models generate data by sampling from a distribution through iterative denoising of noisy intermediate vectors. A forward process is first applied, where noise is gradually added to a clean image  $x_0$  over  $T$  steps. A noisy sample at timestep  $t$  can be expressed as

$$x_t = \sqrt{\bar{\alpha}_t}x_0 + \sqrt{1 - \bar{\alpha}_t}\epsilon, \quad t = 1, \dots, T \quad (1)$$

where  $\epsilon \sim \mathcal{N}(0, \mathbf{I})$ ,  $\alpha_t$  is a predetermined variance schedule, and  $\bar{\alpha}_t = \prod_{i=1}^t \alpha_i$ . The model learns to reverse the forward noising process, which can be expressed as an update step over  $x_t$ ,

$$x_{t-1} = \mu_\theta(x_t, c) + \sigma_t z_t, \quad t = T, \dots, 1 \quad (2)$$

where  $z_t$  are i.i.d standard normal vectors,  $\sigma_t$  is a variance schedule, and  $\mu_\theta(x_t, c)$  is typically parameterized as:

$$\mu_\theta(x_t, c) = \frac{1}{\sqrt{\alpha_t}} \left( x_t - \frac{1 - \alpha_t}{\sqrt{1 - \bar{\alpha}_t}} \epsilon_\theta(x_t, t, c) \right) \quad (3)$$

Here  $\epsilon_\theta(x_t, t, c)$  is the trained noise prediction network, and  $c$  is an optional conditioning context, such as an image prompt embedding.

#### 3.2. DIFFusion

Given an input image  $x_0$ , our goal is to find a fine-grained, discriminative edit that changes a classifier’s prediction. Let  $\mathcal{R}_\theta(\mathbf{z}, c)$  be the recursive application of the denoising diffusion model from Equation (2). Our approach finds these edits by inverting the image  $x_0$ , into a sequence of noise maps,  $\mathbf{z}$ , and manipulating the CLIP embeddings of the original image,  $c = E(x)$ , into a resulting conditioning vector  $\hat{c}$ , before sampling the modified image. We generate the modified image  $\hat{x}_0$  through:

$$\hat{x}_0 = \mathcal{R}_\theta(\mathbf{z}, \hat{c}) \quad (4)$$

Since the diffusion model must generate an image consistent with the original noise maps  $\mathbf{z}$ , and has a conditioning vector  $\hat{c}$  that steers from the source towards the target class, the resulting samples maintain the identity of the original image, but with subtle modifications such that the class label flips.

**Inversion.** We are interested in extracting noise vectors  $\mathbf{z}$ , such that, if used in Equation (2), would recover the original image  $x_0$ . Note that any sequence of  $T + 1$  images

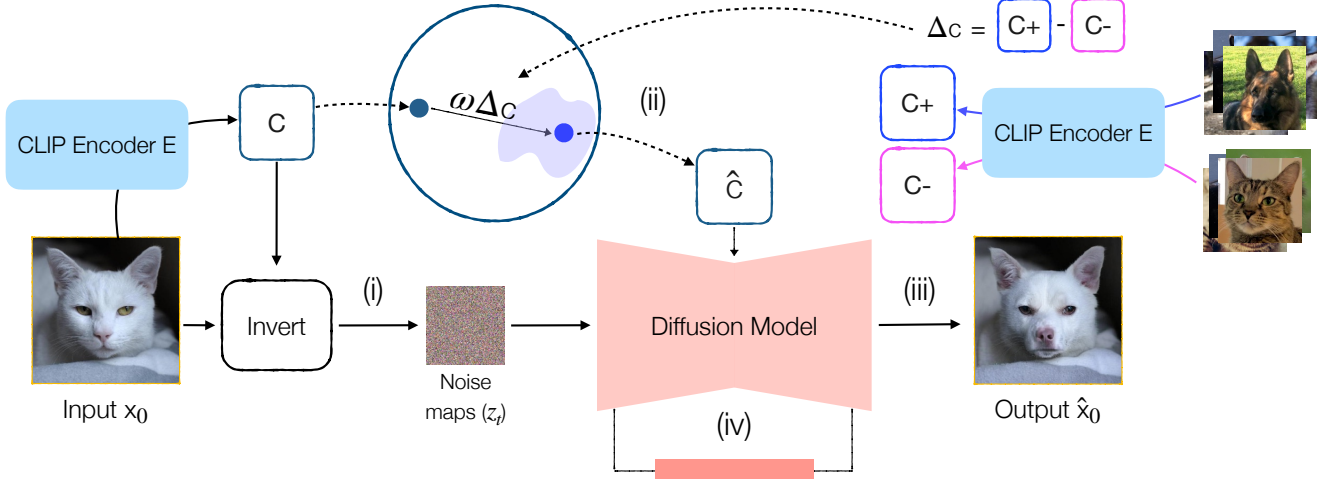


Figure 2. **DIFFusion method.** Our method consists of four parts. (i) Inverting the real image with DDPM-EF to obtain noise maps. (ii) Performing conditioning space arithmetic using positive and negative embeddings obtained from the training set. (iii) Generation via diffusion sampling, starting from the inverted noise conditioning on the manipulated conditioning vector  $\hat{c}$ . (iv) Optional domain tuning, in which we fine-tune the diffusion model for domain adaptation.

$x_0, \dots, x_T$  can be used to extract consistent noise maps for reconstruction by isolating  $z_t$  from Equation (2) as

$$z_t = \frac{x_{t-1} - \mu_\theta(x_t, c)}{\sigma_t}, \quad t = T, \dots, 1 \quad (5)$$

We follow the choice suggested in [22] and compute the noise maps through the standard forward diffusion process Equation (1), but using statistically independently-sampled noise for each timestep. This yields noise maps  $\mathbf{z} = \{z_T, z_{T-1}, \dots, z_1\}$  that are consistent with  $x_0$ .

**Conditioning.** We generate edits that flip the category through arithmetic operations on  $c$ , resulting in  $\hat{c}$ . We apply an additive translation to the conditioning vector  $c = E(x)$ :

$$\hat{c} = c + \omega \Delta c \quad (6)$$

where  $c$  is the CLIP image embedding of the original image,  $\Delta c$  is a direction that moves the class from the original class to the target class, and  $\omega$  is a scaler that varies the direction’s strength. We calculate this translation through the difference of means for each class:

$$\Delta c = \mathbb{E}_{x_p} [E(x_p)] - \mathbb{E}_{x_n} [E(x_n)] \quad (7)$$

such that  $x_p$  is an image of class  $p$  and  $x_n$  is an image of class  $n$  (e.g. positive and negative classes). We normalize all the image embeddings with L2 norm prior to the arithmetic.

**Sampling.** We use  $\hat{c}$  as the conditioning vector for DDPM sampling, paired with the inverted noise maps,  $z$ , to generate the counterfactual image. As suggested in [22], we run

the generation process starting from timestep  $T - T_{skip}$ , where  $T_{skip}$  is a parameter controlling the resemblance to the input image. Therefore, similar to Equation (2), denoting the denoised edited image at timestep  $t$  as  $\hat{x}_t$  we have,

$$\hat{x}_{t-1} = \mu_\theta(\hat{x}_t, \hat{c}) + \sigma_t z_t, \quad t = T - T_{skip}, \dots, 1 \quad (8)$$

This approach allows us to systematically steer the image generation toward the target class by adjusting the manipulation scale  $\omega$ , while maintaining key structural features of the original image through  $T_{skip}$ . Intuitively, a larger  $T_{skip}$  results in fewer denoising steps under the manipulated condition  $\hat{c}$ , leading to greater adherence to the input image.

**Domain Tuning** We use a pre-trained diffusion model [47] that conditions on CLIP image embeddings. When adapting to a new domain, we fine-tune the model using LoRA [21], training only its cross-attention and corresponding projection layers. As discussed in Appendix B.2, we find that domain tuning is beneficial for the Butterfly [52] and Retina [28] datasets, but has minimal impact on the other datasets.

## 4. Experiments

### 4.1. Datasets and Baselines

**Datasets.** We quantitatively benchmark on datasets from diverse domains. We also note the corresponding directions under examination for each dataset. We evaluate on AFHQ [8], CelebA-HQ [31] and KikiBouba [1] as our non-scientific datasets. We also evaluate on three scientific datasets. The first is Retina [28], a dataset of retina cross-sections, both

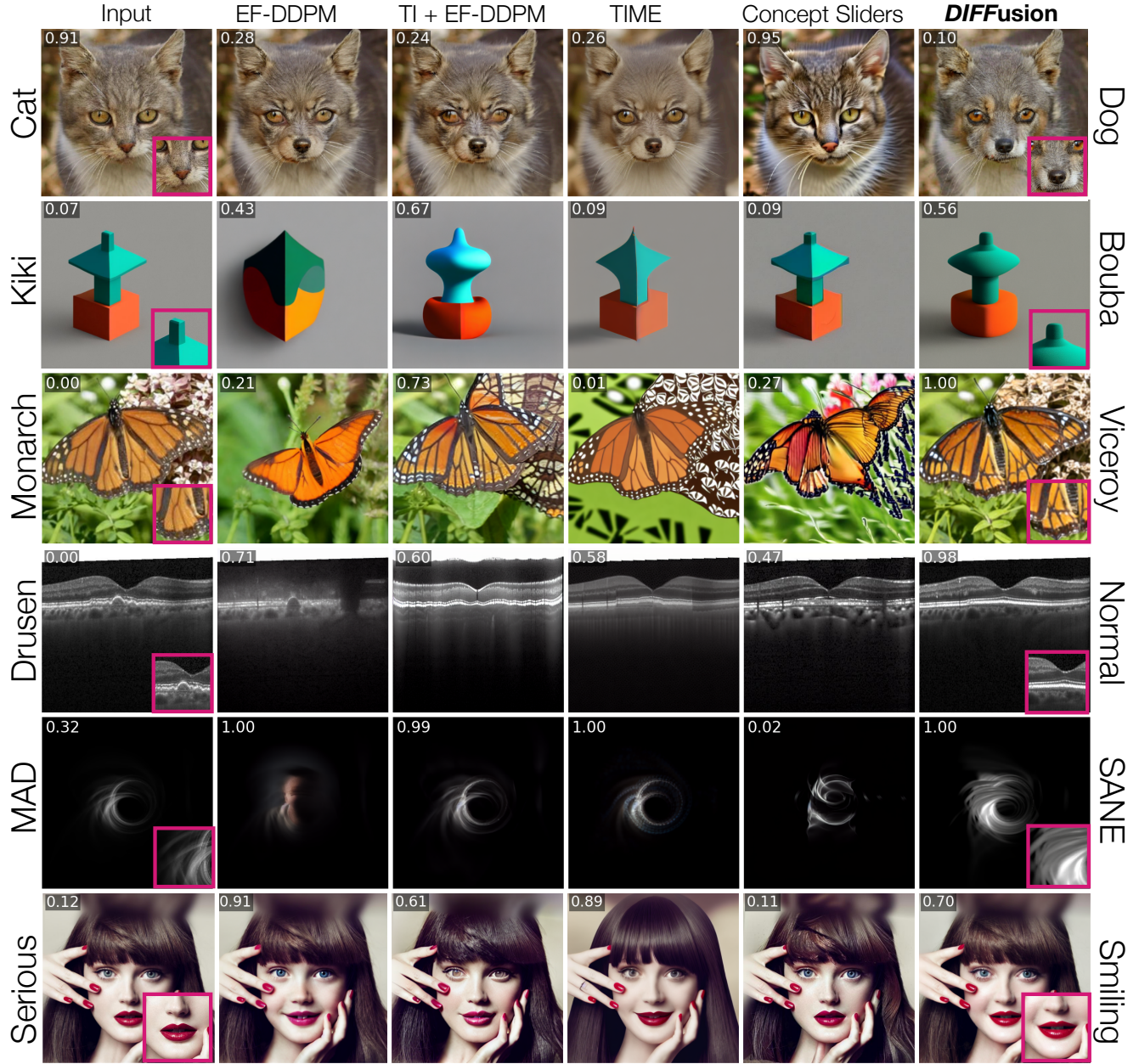


Figure 3. **Qualitative Results.** We present our qualitative results, where each row corresponds to one direction of our binary datasets. The first column contains the inputs, and each subsequent column contains the results from each baseline, with the last column containing the result from *DIFFusion*. The value in the top left corner of the image is the average probability predicted by our ensemble classifiers. In particular, the magnified boxes in the magenta frame show that our method is able to pick up on small discriminative cues. When converting from MAD to SANE, the whisps become amplified and more uniform in brightness. When converting from Drusen to Normal, the small bumps along the cross-section are flattened out. When converting from Monarch to Viceroy, a cross-sectional line is added on the wing.

diseased and healthy. The second is Black Holes, which is a dataset of images taken from fluid simulations of accretion flows around a black hole [54]. The simulations assume general relativistic magnetohydrodynamics (GRMHD) under one of two regimes: magnetically arrested (MAD) or standard and normal evolution (SANE) [26]. Finally,

we also evaluate on Monarch and Viceroy, a fine-grained species classification task. Monarch butterflies evolved to be mimics of Viceroy, and the two species are notoriously difficult to tell apart.

**Baselines.** We use TIME [25] as our counterfactual



Dataset	Class 0 / Class 1
AFHQ [8]	Dog / Cat
KikiBouba [1]	Kiki / Bouba
Retina [28]	Drusen / Normal
Black-Holes	MAD / SANE
Butterfly [52]	Monarch / Viceroy
CelebA-HQ [31]	Smile / No-Smile

Table 1. Datasets and their classification tasks.

baseline, and replace black-box classifier labels with ground truth labels. For editing baselines, we compare against Stable Diffusion [43] with EF-DDPM inversion [22] using class-name prompts. To better accommodate visual concepts, we implemented another baseline that uses Textual Inversion [14] for each class of images and then applies source and target prompts based on the desired edit direction. We term this baseline TI + EF-DDPM. Lastly, we use the visual sliders objective of Concept Sliders [15] that provides a visual counterpart to text-driven attribute edits. To ensure a robust evaluation, we experimented with varying the rank and number of images used for defining the concept direction, selecting the best configuration for each dataset. Since the original method assumes paired data, we adapted it for unpaired settings.

## 4.2. Editing Results

We quantitatively evaluate how well our method can make minimal edits to the image to flip the classifier’s prediction. Since our method can generate different strengths of edits, to pick the minimal edit, we generate 10 edits with varying strengths using the  $T_{skip}$  parameter, as does the TIME baseline [25], testing from highest to lowest  $T_{skip}$ , and select the first edit that flips the classifier prediction while maximizing LPIPS similarity to the original image.

**Metrics.** We evaluate our method using two key metrics. Success Ratio (SR): Also known as Flip-Rate, quantifies the ability of a method to flip an oracle classifier’s decision. The oracle classifier we use is an ensemble of ResNet-18 [17], MobileNet-V2 [46], and EfficientNet-B0 [50], trained on each dataset. LPIPS [58]: Measures the perceptual similarity between the input and generated image, by capturing feature-level difference in a learned embedding space.

**Quantitative Results.** As seen in Table 2, our method achieves the highest SR across all datasets compared to baseline approaches. In terms of LPIPS, it shows significant improvements over previous methods on datasets where language struggles to capture visual details (e.g., Retina, Black-Holes, KikiBouba), unlike datasets with common

objects like AFHQ or CelebA-HQ. It also performs either best or competitively on the remaining natural-image datasets. Additionally, while TI + EF-DDPM improves the same text-based baseline, it still struggles with images that are hard to describe textually, such as Black-Holes.

**Qualitative Results.** In Fig. 3, we present class transitions for all baselines and *DIFFusion*. On familiar datasets like CelebAHQ and AFHQ, our method performs well, similar to baselines. However, its strengths stand out in datasets where language may not fully capture visual details. For KikiBouba, only our method and TI + EF-DDPM round Kiki’s edges, though the baseline changes the original colors, while ours keeps them intact. In the Butterfly dataset, the baselines miss the cross-sectional line, and in the Retina dataset, only our approach removes Drusen while preserving image identity. For the Black-Holes dataset, our method flips the classifier’s prediction with visual features matching SANE’s, even if other methods achieve similar flips. These results suggest our method handles subtle visual nuances particularly well.

## 4.3. Teaching Results

In this section we wish to evaluate how well our method helps people learn to distinguish subtle visual differences between classes.

**User Study Design.** We divided participants into three groups of 10 people each. Group 1 studied only unpaired images. Group 2 studied videos transitioning from original images to counterfactual images generated by the best

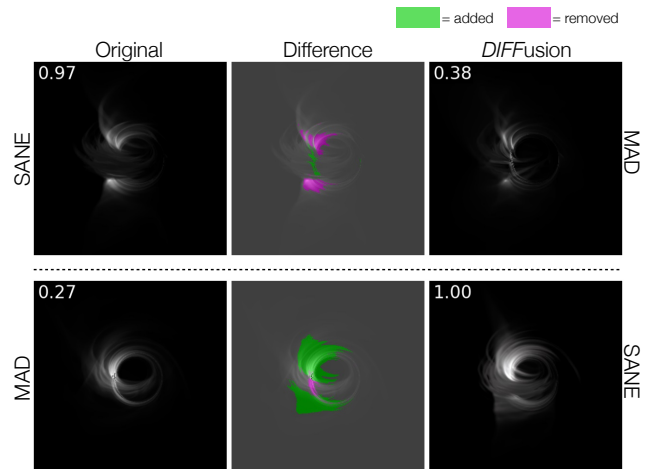


Figure 4. **Original vs. Counterfactual Overlay.** We visualize the difference between the input image and the counterfactual from *DIFFusion*. From SANE to MAD we notice a highlighting of the photon ring (green). From MAD to SANE we notice that the ring becomes less pronounced (magenta), and wisps appear (green).



Table 2. We report the accuracy per dataset, for our method and baselines. SR = Success Ratio, LPIPS = Perceptual Distance. In **bold** are the best results, and in *italic* are the second best results.

Method	AFHQ		KikiBouba		Retina		Black-Holes		Butterfly		Celeba-HQ-Smile	
	SR $\uparrow$	LPIPS $\downarrow$	SR $\uparrow$	LPIPS $\downarrow$	SR $\uparrow$	LPIPS $\downarrow$	SR $\uparrow$	LPIPS $\downarrow$	SR $\uparrow$	LPIPS $\downarrow$	SR $\uparrow$	LPIPS $\downarrow$
EF-DDPM	<b>1.0</b>	<b>0.187</b>	0.68	0.343	0.39	0.272	<i>0.73</i>	0.117	0.86	0.328	<b>1.0</b>	<b>0.104</b>
TI + EF-DDPM	<b>1.0</b>	<i>0.211</i>	<i>0.97</i>	0.332	<i>0.89</i>	0.330	0.5	<b>0.045</b>	<b>1.0</b>	<i>0.289</i>	<b>1.0</b>	0.181
TIME	0.95	0.217	0.17	<b>0.170</b>	0.50	0.358	0.52	0.086	0.13	0.320	0.79	0.166
Concept Sliders	0.49	0.375	0.13	0.206	0.48	<i>0.248</i>	0.53	0.155	0.27	0.362	0.21	0.238
<b><i>DIFFusion</i></b>	<b>1.0</b>	0.245	<b>0.98</b>	<i>0.176</i>	<b>0.98</b>	<b>0.217</b>	<b>1.0</b>	<i>0.076</i>	<b>1.0</b>	<b>0.218</b>	<b>1.0</b>	<i>0.116</i>

baseline. Group 3 studied videos transitioning from original images to counterfactual images generated by our method. Since Groups 2 and 3 viewed transitions from real to edited images, they were also exposed to the unpaired image distribution seen by Group 1. All participants studied their respective materials for 3 minutes to learn to distinguish between the two classes before taking a test. The test required labeling 50 images, evenly distributed with 25 images from each class.

**User Study Results.** We assess *DIFFusion* for teaching via a user study on the Black Holes and Butterfly datasets [52], shown in Figure 5. For Black Holes, unpaired material gave a solid 78% average score, but our counterfactuals boosted this to 90%, with 40% of users hitting near-perfect scores (96%+), surpassing baselines and counterfactuals. For Butterfly, unpaired data led to varied scores, but our counterfactuals raised 9 out of 10 users above 80%, standardizing understanding effectively. P-tests confirm significance: Black Holes ( $p = 0.016$  vs. 0.811 for baseline) and Butterfly ( $p = 0.004$  vs. 0.897 for baseline), both  $p < 0.05$ . Our counterfactuals consistently outperform alternatives, demonstrating the usefulness of our method for teaching humans subtle visual differences.

#### 4.4. Method Analysis

**Varying Dataset Size.** In Fig. 7, we examine the impact of varying the number of images per class on the average LPIPS metric across the test sets. We notice that for most datasets, the LPIPS stops improving at around 50 images.

Table 3. User Study Results - Mean Accuracy (%)

Method	Black Holes	Butterfly	Avg.
	Mean $\pm$ SD	Mean $\pm$ SD	Impr.
Unpaired	78.6 $\pm$ 13.7	61.6 $\pm$ 22.8	—
Baseline	77.2 $\pm$ 11.5	62.8 $\pm$ 16.8	-0.1%
Ours	90.8 $\pm$ 4.8	87.8 $\pm$ 10.4	+19.2%

In Appendix B.4, we show qualitative results as the number of images changes. We notice that as the number of images incorporated into the average embeddings increases, the fidelity to the original image’s identity improves, while subtly altering the features that are distinctive between classes.

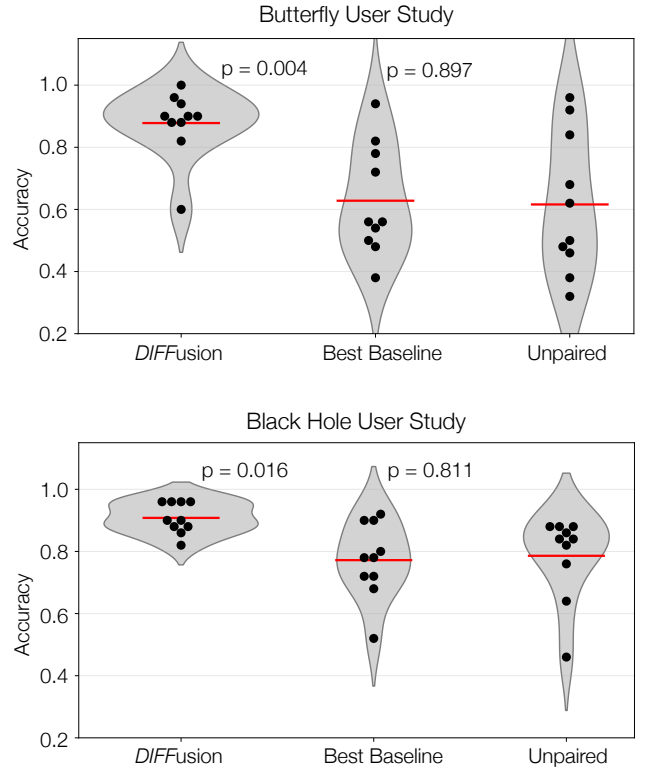


Figure 5. **User Study Results.** We plot the results from user studies across users who studied our counterfactuals, users who studied the best baseline counterfactuals, and users who studied unpaired images. For both Butterfly and Black Hole datasets, we observe that the users who studied our counterfactuals significantly outperformed the other two groups. The violin plots illustrate the distribution of user percentages, where the width of each grey shape represents the density of data points at corresponding percentages.

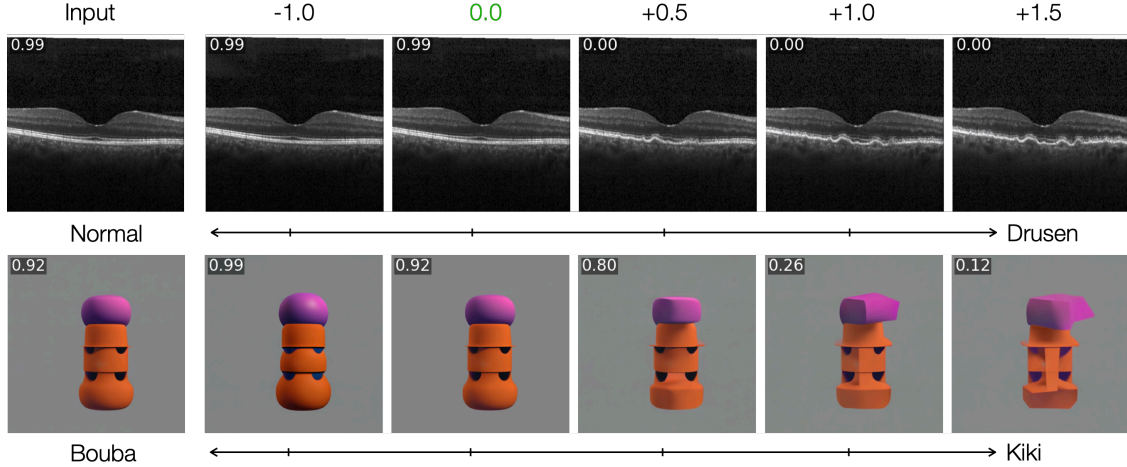


Figure 6. **Interpolation.** By varying the manipulation scale  $\omega \in \{-0.5, 0.0, 0.5, 1.0, 1.5\}$ , we can adjust the manipulation strength, allowing for smooth interpolation between the two classes. Notably, when  $\omega = 0$  (highlighted in green), we can reconstruct the original image while generally preserving the classifier’s probabilities. For a deeper discussion on perfect inversion, refer to Appendix B.3.

**Interpolation.** In Fig. 6, we present qualitative results demonstrating the effects of varying the manipulation scale,  $w$ , on an instance of a Normal retina. The manipulation scale, which can take positive or negative values, modulates the transformation direction. Positive values of  $w$  shift the features toward Drusen from the Normal retina, while negative values make the image smoother.

#### 4.5. Visualizing Dataset Bias

Our method edits images using differences between class mean embeddings, making it sensitive to dataset bias. If

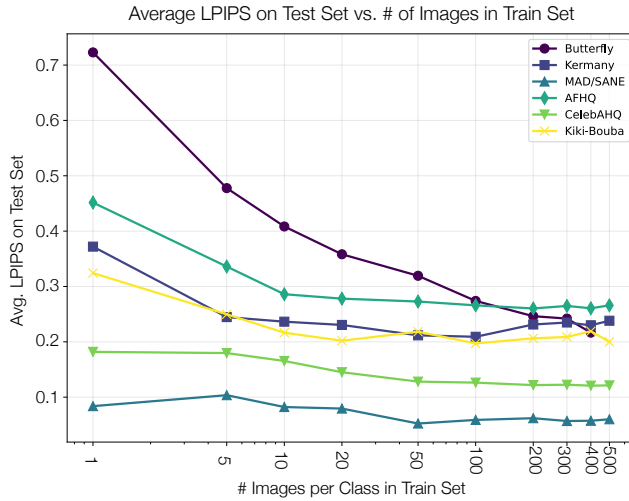


Figure 7. **Varying num. of Images.** Average LPIPS vs. number of images used per class. LPIPS stabilizes around 50 images for most datasets, reflecting improved identity fidelity and subtle class-distinctive feature shifts with increased embedding samples.

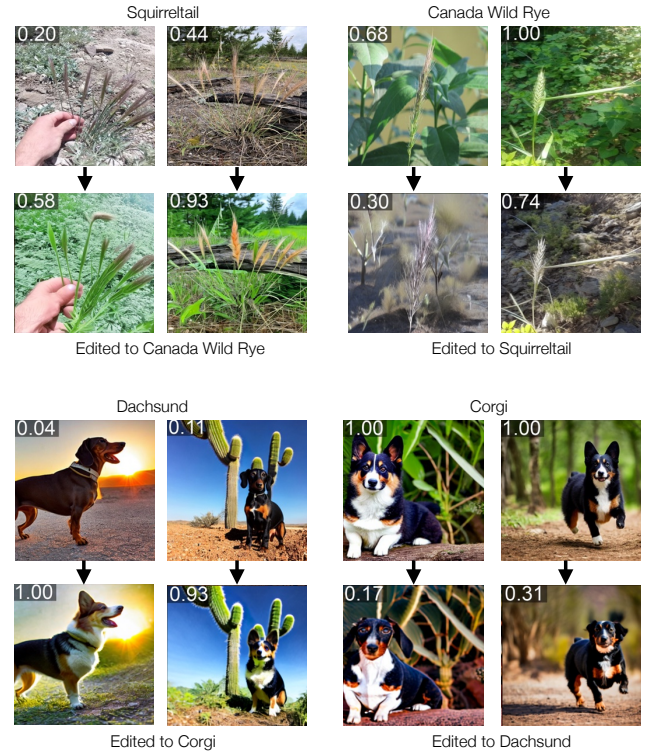


Figure 8. **Dataset Bias.** *DIFFusion* can reveal dataset bias. Squirreltail-to-Canada Wild Rye shifts emphasize environmental backgrounds over plant traits, reflecting iNaturalist’s contextual bias, while Dachshund-to-Corgi edits prioritize foreground dog features, highlighting variable bias impact.

distinguishing features reflect unintended biases rather than targeted traits, edits deviate from our intent. This is both

a limitation—preventing precise control—and a strength, as it visualizes dataset biases, revealing underlying structure. We show how dataset bias is captured by our method in Fig. 8. In iNaturalist [52], counterfactuals from Squirreltail (dry climates) to Canada Wild Rye (humid) shift backgrounds more than plant structure, suggesting environmental bias dominates. Conversely, using the Spawrious [33] dataset, Dachshund-to-Corgi counterfactuals prioritize dog features (e.g., shape, size) over jungle-to-desert backgrounds. We attribute this to stronger foreground differences in dogs and clearer object-background separation, unlike plants blending into settings in iNaturalist data. The effect of dataset bias on edits varies with class prominence and context.

## 5. Discussion and Limitations

*DIFFusion* generates counterfactuals to support visual expertise training across domains with limited data. It reveals dataset biases, often shifting unintended features due to embedding reliance, which limits precise control. Additionally, the arithmetic is very simple: a difference of averages, highlighting a trade-off between flexibility and specificity. Future work could explore disentanglement or guidance mechanisms to enhance edit precision in specialized applications.

**Acknowledgments:** We thank our user study participants and collaborators for their insights. This work is supported by the Carver Mead New Adventures Fund, a Pritzker Award, an AI4Science Amazon Discovery Grant, the NSF AI Institute for Artificial and Natural Intelligence (ARNI), NSF CAREER #2046910, NSF RETTL #2202578, DARPA ECOLE, and a Google Fellowship. Views are ours, not necessarily our sponsors’.

## References

- [1] Morris Alper and Hadar Averbuch-Elor. Kiki or bouba? sound symbolism in vision-and-language models, 2024. 4, 6
- [2] Moab Arar, Rinon Gal, Yuval Atzmon, Gal Chechik, Daniel Cohen-Or, Ariel Shamir, and Amit H. Bermano. Domain-agnostic tuning-encoder for fast personalization of text-to-image models, 2023. 3
- [3] Maximilian Augustin, Yannic Neuhaus, and Matthias Hein. Dig-in: Diffusion guidance for investigating networks – uncovering classifier differences neuron visualisations and visual counterfactual explanations, 2024. 2
- [4] Manuel Brack, Felix Friedrich, Katharina Kornmeier, Linoy Tsaban, Patrick Schramowski, Kristian Kersting, and Apolinário Passos. Ledits++: Limitless image editing using text-to-image models, 2024. 2
- [5] Tim Brooks, Aleksander Holynski, and Alexei A. Efros. Instructpix2pix: Learning to follow image editing instructions, 2023. 2
- [6] Mia Chiquier and Carl Vondrick. Muscles in action. In *Proceedings of the IEEE/CVF International Conference on Computer Vision*, pages 22091–22101, 2023. 3
- [7] Mia Chiquier, Utkarsh Mall, and Carl Vondrick. Evolving interpretable visual classifiers with large language models. In *European Conference on Computer Vision*, pages 183–201. Springer, 2024. 3
- [8] Yunjey Choi, Youngjung Uh, Jaejun Yoo, and Jung-Woo Ha. Stargan v2: Diverse image synthesis for multiple domains. In *2020 IEEE/CVF Conference on Computer Vision and Pattern Recognition (CVPR)*, pages 8185–8194, 2020. 4, 6
- [9] Guillaume Couairon, Jakob Verbeek, Holger Schwenk, and Matthieu Cord. Diffedit: Diffusion-based semantic image editing with mask guidance, 2022. 2
- [10] Gilad Deutch, Rinon Gal, Daniel Garibi, Or Patashnik, and Daniel Cohen-Or. Turboedit: Text-based image editing using few-step diffusion models, 2024. 1
- [11] Prafulla Dhariwal and Alex Nichol. Diffusion models beat gans on image synthesis, 2021. 2
- [12] Lisa Dunlap, Krishna Mandal, Trevor Darrell, Jacob Steinhardt, and Joseph E Gonzalez. Vibecheck: Discover and quantify qualitative differences in large language models. *arXiv preprint arXiv:2410.12851*, 2024. 3
- [13] Karim Farid, Simon Schrodi, Max Argus, and Thomas Brox. Latent diffusion counterfactual explanations, 2023. 2
- [14] Rinon Gal, Yuval Alaluf, Yuval Atzmon, Or Patashnik, Amit H. Bermano, Gal Chechik, and Daniel Cohen-Or. An image is worth one word: Personalizing text-to-image generation using textual inversion, 2022. 2, 6, 1
- [15] Rohit Gandikota, Joanna Materzynska, Tingrui Zhou, Antonio Torralba, and David Bau. Concept sliders: Lora adaptors for precise control in diffusion models, 2023. 2, 6, 1
- [16] Zinan Guo, Yanze Wu, Zhuowei Chen, Lang Chen, Peng Zhang, and Qian He. Pulid: Pure and lightning id customization via contrastive alignment, 2024. 3
- [17] Kaiming He, Xiangyu Zhang, Shaoqing Ren, and Jian Sun. Deep residual learning for image recognition, 2015. 6
- [18] Amir Hertz, Ron Mokady, Jay Tenenbaum, Kfir Aberman, Yael Pritch, and Daniel Cohen-Or. Prompt-to-prompt image editing with cross attention control, 2022. 2
- [19] Jonathan Ho and Tim Salimans. Classifier-free diffusion guidance, 2022. 3, 1, 2
- [20] Jonathan Ho, Ajay Jain, and Pieter Abbeel. Denoising diffusion probabilistic models, 2020. 3
- [21] Edward J. Hu, Yelong Shen, Phillip Wallis, Zeyuan Allen-Zhu, Yuanzhi Li, Shean Wang, Lu Wang, and Weizhu Chen. Lora: Low-rank adaptation of large language models, 2021. 4, 1, 2
- [22] Inbar Huberman-Spiegelglas, Vladimir Kulikov, and Tomer Michaeli. An edit friendly ddpm noise space: Inversion and manipulations, 2024. 3, 4, 6, 1, 2
- [23] Guillaume Jeanneret, Loïc Simon, and Frédéric Jurie. Diffusion models for counterfactual explanations, 2022. 2
- [24] Guillaume Jeanneret, Loïc Simon, and Frédéric Jurie. Adversarial counterfactual visual explanations, 2023.

- [25] Guillaume Jeanneret, Loïc Simon, and Frédéric Jurie. Text-to-image models for counterfactual explanations: A black-box approach. In *Proceedings of the IEEE/CVF Winter Conference on Applications of Computer Vision (WACV)*, pages 4757–4767, 2024. 2, 5, 6, 1
- [26] Hong-Xuan Jiang, Yosuke Mizuno, Christian M Fromm, and Antonios Nathanail. Two-temperature grmhd simulations of black hole accretion flows with multiple magnetic loops. *Monthly Notices of the Royal Astronomical Society*, 522(2): 2307–2324, 2023. 5
- [27] John Jumper, Richard Evans, Alexander Pritzel, Tim Green, Michael Figurnov, Olaf Ronneberger, Kathryn Tunyasuvunakool, Russ Bates, Augustin Žídek, Anna Potapenko, et al. Highly accurate protein structure prediction with alphafold. *nature*, 596(7873):583–589, 2021. 3
- [28] Daniel S Kermany, Michael Goldbaum, Wenjia Cai, Carolina CS Valentim, Huiying Liang, Sally L Baxter, Alex McKeown, Ge Yang, Xiaokang Wu, Fangbing Yan, et al. Identifying medical diagnoses and treatable diseases by image-based deep learning. *cell*, 172(5):1122–1131, 2018. 2, 4, 6
- [29] Black Forest Labs. Flux. <https://github.com/black-forest-labs/flux>, 2024. 2, 3
- [30] Oran Lang, Yossi Gandelsman, Michal Yarom, Yoav Wald, Gal Elidan, Avinatan Hassidim, William T. Freeman, Phillip Isola, Amir Globerson, Michal Irani, and Inbar Mosseri. Explaining in style: Training a gan to explain a classifier in stylespace, 2021. 2
- [31] Cheng-Han Lee, Ziwei Liu, Lingyun Wu, and Ping Luo. Maskgan: Towards diverse and interactive facial image manipulation. In *2020 IEEE/CVF Conference on Computer Vision and Pattern Recognition (CVPR)*, pages 5548–5557, 2020. 4, 6
- [32] Ce Liu, Antonio Torralba, William T Freeman, Frédo Durand, and Edward H Adelson. Motion magnification. *ACM transactions on graphics (TOG)*, 24(3):519–526, 2005. 3
- [33] Aengus Lynch, Gbètondji J-S Dovonon, Jean Kaddour, and Ricardo Silva. Spawrious: A benchmark for fine control of spurious correlation biases, 2023. 9
- [34] Utkarsh Mall, Cheng Perng Phoo, Mia Chiquier, Bharath Hariharan, Kavita Bala, and Carl Vondrick. Disciple: Learning interpretable programs for scientific visual discovery. *arXiv preprint arXiv:2502.10060*, 2025. 3
- [35] Chenlin Meng, Yutong He, Yang Song, Jiaming Song, Jiajun Wu, Jun-Yan Zhu, and Stefano Ermon. Sdedit: Guided image synthesis and editing with stochastic differential equations, 2022. 2
- [36] Ron Mokady, Amir Hertz, Kfir Aberman, Yael Pritch, and Daniel Cohen-Or. Null-text inversion for editing real images using guided diffusion models, 2022. 3
- [37] Alexander Quinn Nichol, Prafulla Dhariwal, Aditya Ramesh, Pranav Shyam, Pamela Mishkin, Bob McGrew, Ilya Sutskever, and Mark Chen. GLIDE: Towards photorealistic image generation and editing with text-guided diffusion models. In *Proceedings of the 39th International Conference on Machine Learning*, pages 16784–16804. PMLR, 2022. 2
- [38] Tae-Hyun Oh, Ronnachai Jaroensri, Changil Kim, Mohamed Elgharib, Frédo Durand, William T Freeman, and Wojciech Matusik. Learning-based video motion magnification. In *Proceedings of the European conference on computer vision (ECCV)*, pages 633–648, 2018. 3
- [39] Gaurav Parmar, Krishna Kumar Singh, Richard Zhang, Yijun Li, Jingwan Lu, and Jun-Yan Zhu. Zero-shot image-to-image translation, 2023. 2, 3
- [40] Aditya Ramesh, Prafulla Dhariwal, Alex Nichol, Casey Chu, and Mark Chen. Hierarchical text-conditional image generation with clip latents, 2022. 2, 3
- [41] Anton Razzhigaev, Arseniy Shakhmatov, Anastasia Maltseva, Vladimir Arkhipkin, Igor Pavlov, Ilya Ryabov, Angelina Kuts, Alexander Panchenko, Andrey Kuznetsov, and Denis Dimitrov. Kandinsky: an improved text-to-image synthesis with image prior and latent diffusion, 2023. 3, 2
- [42] Pau Rodriguez, Massimo Caccia, Alexandre Lacoste, Lee Zamparo, Issam Laradji, Laurent Charlin, and David Vazquez. Beyond trivial counterfactual explanations with diverse valuable explanations, 2021. 2
- [43] Robin Rombach, Andreas Blattmann, Dominik Lorenz, Patrick Esser, and Björn Ommer. High-resolution image synthesis with latent diffusion models. In *2022 IEEE/CVF Conference on Computer Vision and Pattern Recognition (CVPR)*, pages 10674–10685, 2022. 2, 6, 1
- [44] Bernardino Romera-Paredes, Mohammadamin Barekatain, Alexander Novikov, Matej Balog, M Pawan Kumar, Emilien Dupont, Francisco JR Ruiz, Jordan S Ellenberg, Pengming Wang, Omar Fawzi, et al. Mathematical discoveries from program search with large language models. *Nature*, 625 (7995):468–475, 2024. 3
- [45] Chitwan Saharia, William Chan, Saurabh Saxena, Lala Li, Jay Whang, Emily Denton, Seyed Kamyar Seyed Ghasemipour, Burcu Karagol Ayan, S. Sara Mahdavi, Rapha Gontijo Lopes, Tim Salimans, Jonathan Ho, David J Fleet, and Mohammad Norouzi. Photorealistic text-to-image diffusion models with deep language understanding, 2022. 2
- [46] Mark Sandler, Andrew Howard, Menglong Zhu, Andrey Zhmoginov, and Liang-Chieh Chen. Mobilenetv2: Inverted residuals and linear bottlenecks, 2019. 6
- [47] Arseniy Shakhmatov, Anton Razzhigaev, Aleksandr Nikolich, Vladimir Arkhipkin, Igor Pavlov, Andrey Kuznetsov, and Denis Dimitrov. kandinsky 2.2. <https://github.com/ai-forever/Kandinsky-2>, 2023. 4, 1
- [48] Bartłomiej Sobieski and Przemysław Biecek. Global counterfactual directions, 2024. 2
- [49] Jiaming Song, Chenlin Meng, and Stefano Ermon. Denoising diffusion implicit models, 2022. 3, 2
- [50] Mingxing Tan and Quoc V. Le. Efficientnet: Rethinking model scaling for convolutional neural networks, 2020. 6
- [51] Narek Tumanyan, Michal Geyer, Shai Bagon, and Tali Dekel. Plug-and-play diffusion features for text-driven image-to-image translation. In *Proceedings of the IEEE/CVF Conference on Computer Vision and Pattern Recognition*, pages 1921–1930, 2023. 2
- [52] Grant Van Horn, Oisín Mac Aodha, Yang Song, Yin Cui, Chen Sun, Alex Shepard, Hartwig Adam, Pietro Perona, and Serge Belongie. The inaturalist species classification and detection dataset. In *Proceedings of the IEEE conference on*



*computer vision and pattern recognition*, pages 8769–8778, 2018. [4](#), [6](#), [7](#), [9](#)

- [53] Bram Wallace, Akash Gokul, and Nikhil Naik. Edict: Exact diffusion inversion via coupled transformations, 2022. [3](#)
- [54] George N Wong, Ben S Prather, Vedant Dhruv, Benjamin R Ryan, Monika Mościbrodzka, Chi-kwan Chan, Abhishek V Joshi, Ricardo Yarza, Angelo Ricarte, Hotaka Shiokawa, et al. Patoka: Simulating electromagnetic observables of black hole accretion. *The Astrophysical Journal Supplement Series*, 259(2):64, 2022. [5](#)
- [55] Chen Henry Wu and Fernando De la Torre. Unifying diffusion models’ latent space, with applications to cyclediffusion and guidance, 2022. [3](#), [2](#)
- [56] Hao-Yu Wu, Michael Rubinstein, Eugene Shih, John Gutttag, Frédo Durand, and William Freeman. Eulerian video magnification for revealing subtle changes in the world. *ACM transactions on graphics (TOG)*, 31(4):1–8, 2012. [3](#)
- [57] Hu Ye, Jun Zhang, Sibor Liu, Xiao Han, and Wei Yang. Ip-adapter: Text compatible image prompt adapter for text-to-image diffusion models, 2023. [3](#)
- [58] Richard Zhang, Phillip Isola, Alexei A Efros, Eli Shechtman, and Oliver Wang. The unreasonable effectiveness of deep features as a perceptual metric. In *CVPR*, 2018. [6](#)
- [59] Xiaojin Zhu. Machine teaching: An inverse problem to machine learning and an approach toward optimal education. In *Proceedings of the AAAI conference on artificial intelligence*, 2015. [3](#)

# Teaching Humans Subtle Differences with *DIF*Fusion

## Supplementary Material

### A. Implementation Details

#### A.1. Method Implementation Details

We utilize the diffusion decoder from [47] and optionally fine-tune LoRA [21] weights on either subsets or the full dataset as discussed in Section 4.4. For fine-tuning, we set the LoRA rank to 4, the LoRA scaling factor to  $\alpha = 8$  and use a base learning rate of 0.003.

For inversion, we adapt the edit-friendly DDPM inversion scheme [22] to our diffusion decoder. Specifically, we use CFG [19] in both inversion and generation, motivated by [10, 22]. We first aim to find guidance scale parameters that achieve perfect reconstruction, and then use these scales for our method. This process is further discussed in Appendix B.3.

To generate counterfactuals, we manipulate the CLIP image space using Equation (6), adjusting the manipulation guidance scale per dataset ( $\omega = 1.0$  for AFHQ,  $\omega = 2.0$  for the rest of the datasets).

#### A.2. Baselines Implementation Details

As described in Section 4.1 we compare our method against the following baselines: TIME [25], Stable Diffusion [43] with EF-DDPM inversion [22], once using class names as text prompts, and once using learned textual embeddings of a group of each class’ images through Textual Inversion [14]. Lastly we also compare to Concept Sliders [15]. We used the following third-party implementation in this project:

- TIME: [25]. Instead of using their classifier’s labels to group the data into two classes, we used the ground-truth labels. Additionally, to perform the evaluations, we used our own ensemble classifiers. [official implementation](#).
- EF-DDPM [22]: [official implementation](#). For the prompt-based baseline, we use class names as prompts of the form “a photo of a CLASS-NAME”, where CLASS-NAME can be “cat”, “viceroy”, “drusen”, etc. For the scientific datasets we also include an identifier of the form “Butterfly”, “Black Hole”, “Retina”. For the textual-inversion-based baseline (TI + EF-DDPM), we first invert each class of images into a newly added token and save when optimization is done. Then, we use the source-class token as the inversion prompt, and the target-class token as the generation prompt.
- Concept Sliders [15]: [official implementation](#). We built on the official implementation of official implementation, utilizing their Visual Concept Sliders and image editing script. While their approach assumes paired data, we found that unpaired data performs well on datasets

with well-aligned classes, such as AFHQ. Conversely, for datasets with less alignment, like Butterfly, training with fewer images—ranging from 5 to 20—slightly improved results. To optimize performance, we varied both the number of training images and the LoRA rank for each dataset, evaluating combinations to select the best one per dataset.

As discussed in Section 4.2, our evaluation algorithm starts by adjusting parameters that have the strongest manipulation effect first (e.g. guidance scales,  $T_{skip}$ , and manipulation scale), and stops as soon as a flip occurs, logging the generated image along with the parameters that caused the flip. If no flip is achieved, we apply the final set of parameters designed to induce the most significant edit.

#### A.3. User Study Details

Group 1 studied a folder of unpaired images for 3 minutes. This folder contained images of both classes, with the label of the class written on top of the image. Group 2 studied the unpaired image folder for 1 minute, the counterfactuals generated by the best baseline from Class 0 to Class 1 for another minute, and finally the counterfactuals generated by the best baseline from Class 1 to class 0 for a minute. Group 3 followed the same protocol as Group 2, except with our counterfactuals instead. For both Butterfly and Black hole, the best baseline was TI + DDPM-EF, according to LPIPS. We only showed counterfactuals where the class flipped.

The participants of the user studies were undergraduates and graduates who volunteered in exchange for baked goods. The supplementary material contains videos of the study material for Group 3, for both the black hole and the butterfly dataset. No user had any prior knowledge about either of the datasets before studying the material and taking the test.

### B. Additional Experiments

#### B.1. SR vs. LPIPS Curves

In Figure 9 we plot the Success Ratio vs. LPIPS curves for our method compared to the best baseline - TI + EF-DDPM, rather than choosing a single set of parameters which is required to report Table 2. Since both use the same inversion technique, we create these curves by varying the  $T_{skip}$  parameter. A higher AUC generally indicates a better tradeoff between classifier flip-rate and similarity to input images for each dataset. Our method outperforms the best baseline across all datasets while achieving comparable performance on AFHQ.

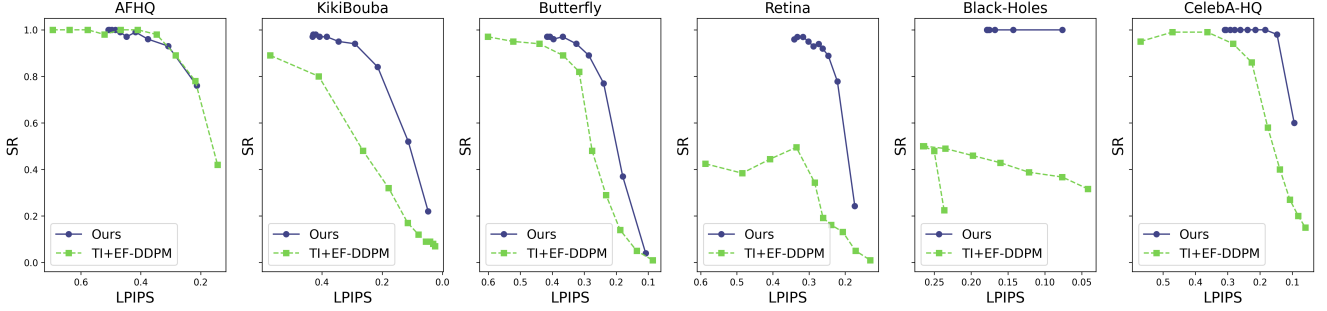


Figure 9. **Success Ratio (SR) vs. LPIPS curves.** As discussed in Appendix B.1, we fix the guidance scales for each method, and the manipulation scale  $\omega$  for ours according to Appendix A. We then vary  $T_{skip}$  in increments of 0.1 within the range  $[0.0, 0.9]$ , where  $T_{skip}$  represents the percentage of timesteps skipped relative to the total denoising steps.

## B.2. Results w/o Domain Tuning

As discussed in Appendix A.1, we begin by fine-tuning a LoRA adapter [21], applied to the cross-attention and their linear projection weights, using a simple loss at random timesteps  $t$ , i.e:

$$\mathcal{L}_{simple} = \mathbb{E}_{x, \epsilon, t} [\|\epsilon - \epsilon_{\theta}(x_t, t, c)\|_2^2]$$

where the prompts  $c$  are derived from image embeddings of training set examples. To obtain the best weights, we log SR and LPIPS scores on a small validation set at the end of each epoch. In certain datasets, fine-tuning has minimal to no impact on the overall results. This suggests that, in some cases, the prior learned by the pre-trained diffusion model is sufficiently strong to produce meaningful edits when conditioned on a manipulated CLIP image embedding. The results of this analysis are presented in Table 4, where we observe that domain tuning plays a crucial role in datasets like Retina and Butterfly, while having a lesser effect on others.

## B.3. Perfect Inversion

Perfect reconstruction can be achieved when the same conditioning prompt is used during both inversion and sampling. In this case, we hope that the original image is fully reconstructed. However, DDIM [49] introduces small errors at each timestep, making exact reconstruction challenging, especially with a limited number of timesteps or within the classifier-free guidance framework [19]. Recent works [4, 22, 55] focus on non-deterministic DDPM inversion and have demonstrated perfect image reconstruction when applied to Stable Diffusion [43]. Since we are using an image-conditioned diffusion decoder from the Kandinsky model family [41], we first explore the choice of guidance scales required to achieve perfect reconstruction while using CFG in both inversion and generation. While perfect reconstruction does not necessarily guarantee a useful editing space, poor reconstruction from the start is likely to cause significant deviations from the source image—an undesirable outcome when generating counterfactuals. Figure 10 illustrates

this effect, showing that using equal guidance terms in inversion and sampling results in good reconstruction, which starts to degrade when inversion guidance scale,  $\omega_{src}$ , and target guidance scale,  $\omega_{tar}$ , are larger than 4.

## B.4. Varying Dataset Size Results

As described in Section 4.4, and in Figure 7, we demonstrate the effect of varying the number of images we have access to for applying *DIFFusion*. In this section, we show examples of generated counterfactuals per number of images in access,  $N$ , as shown in Figures 11 to 13. We show the grids with increasing number of images so long as the results continue to improve.

## B.5. Results

Table 4. **Results without Domain Tuning.** We evaluate our method without fine-tuning on each dataset, measuring performance using Success Ratio (SR) and perceptual distance (LPIPS). Compared to Table 2, we observe substantial improvements in both SR and similarity for the Retina and Butterfly datasets, as well as noticeable gains in reconstruction for Black-Holes and KikiBouba. However, the impact is minimal on the most natural-image datasets, AFHQ and CelebA-HQ. This suggests that the prior learned by the pre-trained diffusion model is strong enough to generate meaningful edits for these datasets without additional fine-tuning.

Method	AFHQ		KikiBouba		Retina		Black-Holes		Butterfly		Celeba-HQ-Smile	
	SR $\uparrow$	LPIPS $\downarrow$	SR $\uparrow$	LPIPS $\downarrow$	SR $\uparrow$	LPIPS $\downarrow$	SR $\uparrow$	LPIPS $\downarrow$	SR $\uparrow$	LPIPS $\downarrow$	SR $\uparrow$	LPIPS $\downarrow$
Ours	1.0	0.249	0.98	0.2014	0.515	0.454	0.980	0.119	0.31	0.344	1.0	0.123

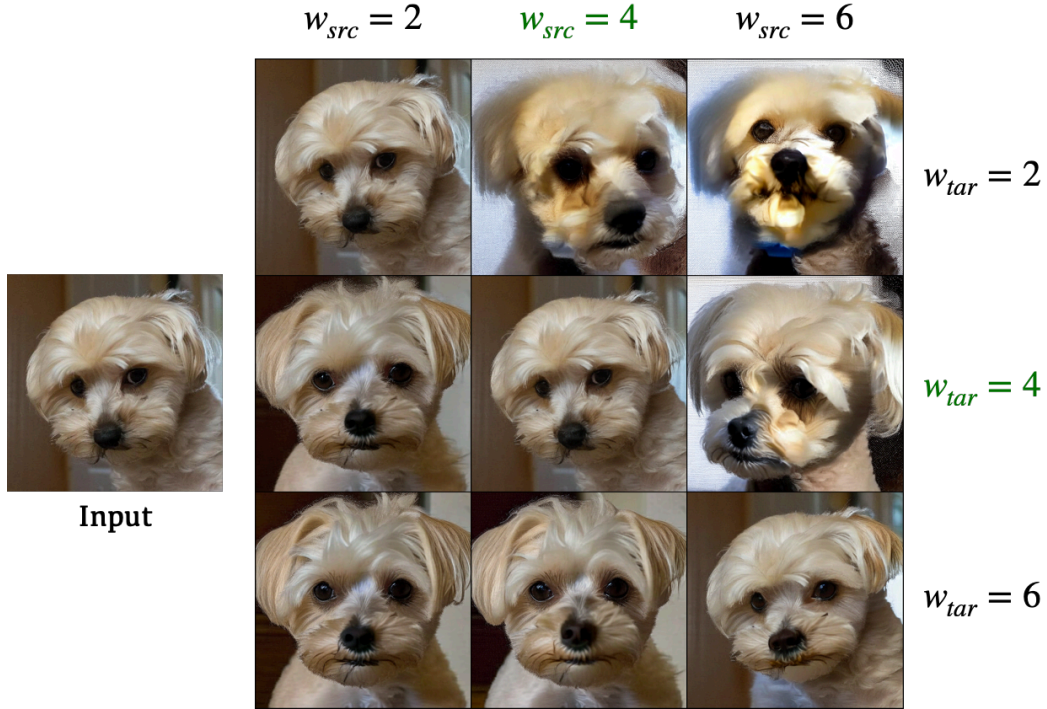


Figure 10. Perfect Inversion.





Figure 11. Varying Number of Images for AFHQ.



Figure 12. Varying Number of Images for Butterfly.



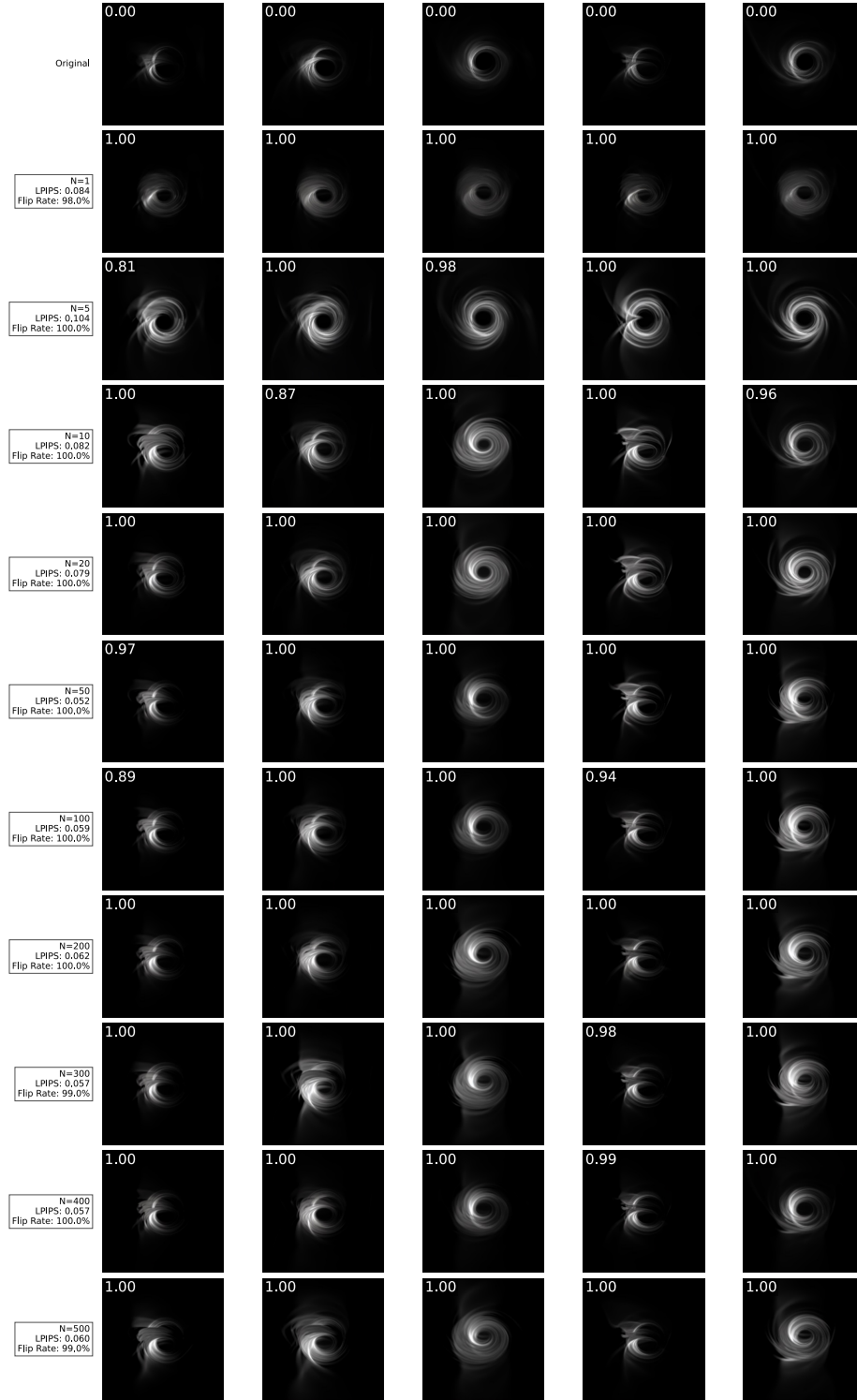


Figure 13. Varying Number of Images for MAD/SANE.